17th World Conference on Earthquake Engineering, 17WCEE
Sendai, Japan - September 13th to 18th 2020

HYDRODYNAMIC LOADING ON PIPELINES DURING EXTREME COASTAL FLOODING EVENTS

I. Nistor[(1)], B. Ghodoosipour[(2)], A. Mohammadian[(3)], T. Takabatake[(4)], T. Shibayama[(5)]

[(1)] *Professor, Dept. of Civil Engineering, University of Ottawa, Canada, inistor@uottawa.ca*
[(2)] *PhD student, Dept. of Civil Engineering, University of Ottawa, Canada, bghod068@uottawa.ca*
[(3)] *Professor, Dept. of Civil Engineering, University of Ottawa, Canada, amohamma@uottawa.ca*
[(4)] *Assistant Professor, Waseda Research Institute for Science and Engineering, Waseda University, Tokyo, Japan, takabatake@aoni.waseda.jp*
[(5)] *Professor, Dept. of Civil and Environmental Engineering, Waseda University, Tokyo, Japan, shibayama@waseda.jp*

Abstract

Adequate design of pipelines used for oil, gas, water and wastewater transmission is essential not only for their proper operation but particularly to avoid failure and the possible extreme consequences induced. This is even more drastic in nearshore environments, where pipelines are potentially exposed to extreme hydrodynamic events, such as tsunami-induced inundation or storm surges. The American Society of Civil Engineers (ASCE), in its ASCE/SEI7 Chapter 6 [1] on Tsunami Loads and Effects which is the new standard for tsunami impacts and loading, specifically stresses the need to study loads on pipelines located in tsunami-prone areas. To address this issue, this study is the first of its kind to investigate loading on pipelines due to tsunami-like bores. A comprehensive program of physical model experiments was conducted in the Dam-Break Hydraulic Flume at the University of Ottawa, Canada. The tests simulated on-land tsunami flow inundation propagating over a coastal plain. This allowed to record and investigate the hydrodynamic forces exerted on the pipe due to the tsunami-like, dam-break waves. Different pipe configurations, as well as various flow conditions, were tested to investigate their influence on exerted forces and moments. The goal of this study was to propose, in premiere, based on the results of this study, resistance and lift coefficients which could be used for the design of pipelines located in tsunami-prone areas. The study proposes specific values for drag coefficients in the case of a transient tsunami-like coastal flow for different relative gap ratios (e/D) and pipe submergence conditions. Different pipe configurations as well as various flow conditions were tested to investigate their influence on exerted forces and moments. This results and analysis focused on measuring and analyzing the forces induced by extreme hydrodynamic events on submerged and above-ground pipelines. The ultimate goal of this study is to propose, based on the results of this study, resistance and lift coefficients to be used for the design of pipelines located in tsunami-prone areas.

Keywords: pipelines; hydrodynamic loading, ASCE7-Chapter 6; tsunami; bores; experimental

1. Introduction

Over the past several decades, extreme tsunami and storm surge events demonstrated the danger posed to coastal communities by natural disasters. The number of people experiencing such catastrophic events have increased due to climate change and increasing population which has led to an increased interest of research around the topic. The need to study such events in the context of hydrodynamics and their interaction with different structures is significant to mitigate such future disastrous events. Coastal hazards, such as tsunamis storm surges and typhoons, can generate extremely turbulent waves, breaking into the coastal areas and destroying structures along their path. Moreover, sudden dam failure incidents can also cause similar impacts on their vulnerable downstream infrastructures. Understanding the dynamics of breaking waves, turbulent and transient currents as well as wave-structure interaction is difficult and complex. This is due to the problem being non-linear, time-dependent and its common involvement of turbulent multi-phase processes.

Many researchers conducted post-event field surveys of the recent catastrophic events, such as the 2004 Indian Ocean and 2011 Tohoku Tsunami. Results from such detailed surveys are decent sources of hydrodynamics investigations. Field survey results in Khao Lak, Thailand, estimated inundation heights between 4 to 7 m and wave front celerities between 6 to 8 m/s [2]. Investigations by the Japanese Port and Airport Research Institute (PARI) during the 2011 Tohoku Tsunami in Japan recorded inundation height of up to 15 m in the city of Onagawa. Onshore inundation velocities up to 10 to 13 m/s were also observed near Sendai airport. [4] performed a field survey using video-processing in Kasennuma Bay and estimated inundation depths up to 9 m, flow velocities of up to 11 m/s and Froude Number's around 1

In this study, dam-break wave generated using a swing gate was used as a representation for enormously turbulent waves generated in extreme events, such as tsunamis. Several researchers have characterized dam break wave surging over a dry bed. Among them Ritter [5], Henderson [6] and Chanson [7] developed solutions for the wave profile.

Investigations of the existing research in the context of extreme flow condition impact on different structures, reveals a clear absence of research on the impact of transient tsunami-like waves on horizontal pipelines. Catastrophic events, such as the 2011 Tohoku Tsunami in Japan and the 2012 Typhoon Haiyan in the Philippines, have raised an increased interest of research groups to re-evaluate existing design and safety standards in a way that they would consider effects of such extreme events. The American Society of Civil Engineers (ASCE), through its ASCE7 Tsunami Loads and Effects Committee, has developed a new standard for tsunami impacts and loading, [1]. Amongst the potential effects of such extreme events on infrastructure, the standard has emphasized the need to investigate tsunami loads on pipelines.

The main goal of this study is a better understanding of the extreme hydrodynamic loading on pipelines. The specific objectives of the presented study as part one of a two-part paper are to study the flow hydrodynamics of the dam-break waves. The following questions were examined in this study:

- What are the flow characteristics (time-history of the wave surface profile and flow velocity) for dam break waves propagating over dry bed condition for different wave heights?
- How are flow characteristics altered in the case of the dam-break wave propagation over a wet bed condition and how are these characteristics changing when wave height changes and/or when the still water depth of the wet bed varies?
- How do flow conditions get influenced by the presence of a horizontal cylindrical pipe immersed in the flow under both dry and wet bed conditions?

2. Experimental Program

A comprehensive experimental program was developed and conducted in the Dam-break Flume in the Hydraulics Laboratory at the University of Ottawa (Canada). Experiments were performed at a 1:25 scale. Scaling was done considering Froude similitude. The flume is 30.1 m in length, 1.5 m in width, and 0.5 m in height. A volume of water was impounded behind a swinging gate installed in the flume to form an upstream reservoir with a length of 21.55 m reservoir and variable water depths. The dam-break waves were generated by the rapid opening of the swinging gate. According to a study conducted in the same flume by Stolle et al., [2018], the non-dimensional gate opening time, $T_0=(t/\sqrt{(g.h)})$ (t being the physical gate opening time, h being the impoundment depth) is dependent on the initial impoundment depth with an approximately linear relationship as:

$$T_0=1.47-1.19h \quad (1)$$

With the range of impoundment depths tested in this study the non-dimensional gate opening time was in the range of $0.875<T_0<1.113$. Therefore, the range of T_0, satisfied the Lauber and Hager [8] criterion for acceptable non-dimensional gate opening time for a dam-break wave as less than 1.41. A vertically-moving steel gate located at the downstream end of the flume ensured the control of the water level downstream of the swing gate and enabled thus the formation of wet bed conditions with different water depths. The pipe model which was tested was made of cold rolled steel, 10 cm in diameter and 1.47 m in length, installed

horizontally and transversally across the flume at x = 5.6 m downstream of the gate. Schematics of the flume together with various experimental parameters are shown in Figure 1.

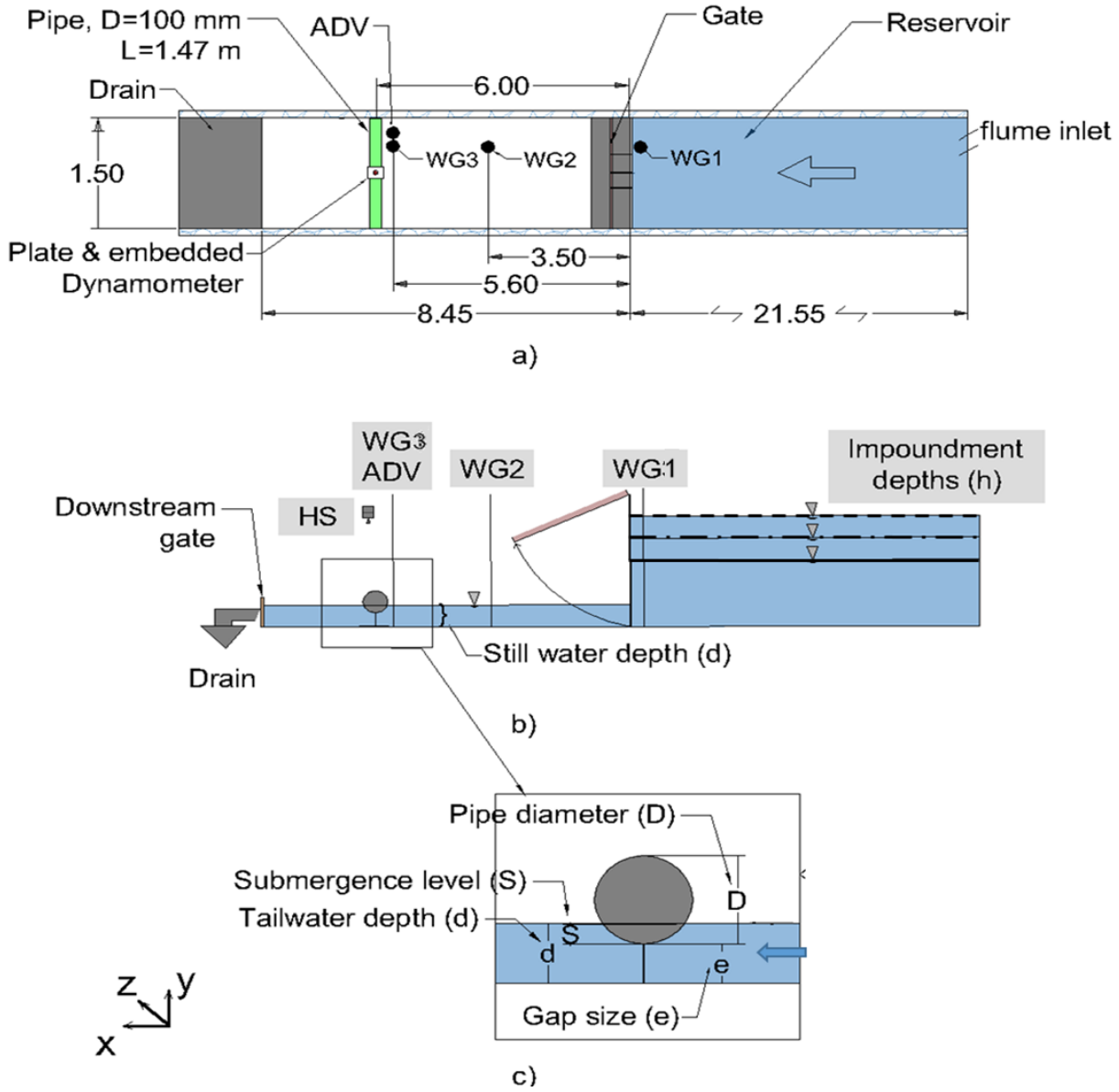

Fig. 1 - Flume and instrumentation sketch, (unless otherwise specified, all dimensions are in m). a) Plan view, b) Side view, c) Close view, pipe and experimental parameters.

2.1 Instrumentation

Various instrumentation was used to record the time history of the water surface (capacitance wave gages and ultrasonic wave gages), flow velocity (Acoustic Doppler Velocimeters – ADVs), and the time history of the forces exerted on the pipes. Pictures of the experimental setting are shown in Figure 2.

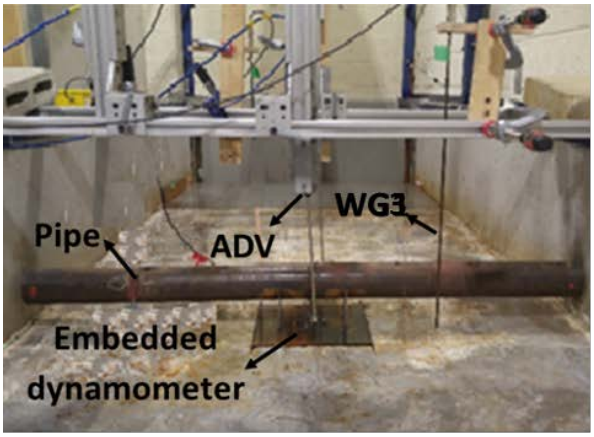

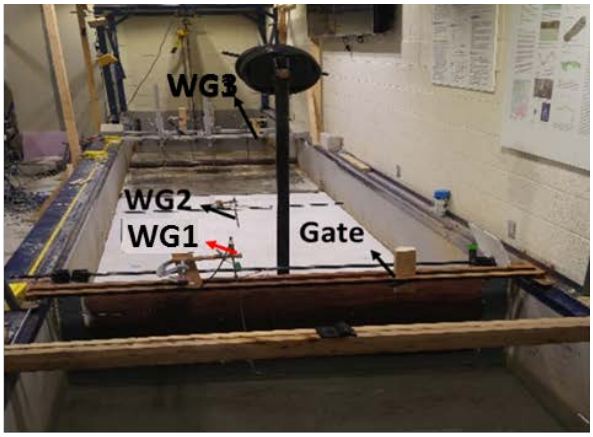

a) b)

Fig. 2 - a) Downstream view, pipe, dynamometer, ADV and wave gauge, b) downstream view, gate

To record the time-history of the water level, three wave gauges (RBR WG-50, capacitance-type, ±0.002 accuracy) were installed at different locations along the flume. The first wave gauge (WG3) was installed upstream of the gate (x = -0.04 m) and was used to determine the opening time of the gate. The other two wave gauges were located at x = 3.5 m (WG2) and x = 5.6 m (WG1) downstream of the gate. The wave gauges sampling rate for data collection was 300 Hz.

A high-resolution acoustic Doppler velocimeter (ADV) (Vectrino, ± 1 mm/s accuracy, 2.5 m/s measurement range) was used for velocity measurements in free stream flow. The velocity was used in the estimation of the drag and lift coefficients. The ADV was able to measure 3-D water velocities using coherent Doppler processing technology. In this study, a side looking ADV was used. The ADV's sampling rate was set to 200 Hz. The instrument was located at x = 5.6 m, 0.10 m upstream of the outer edge of the pipe. To derive the velocity profile, each experiment with the specific configuration was repeated three times and ADV was moved vertically to different depth: (1) the highest water level; (2) the location where the center-axis of the pipe cross section was placed and 0.03 m above the flume bed.

To record the time-history of the forces exerted on the pipe, a 6 degree of freedom (DOF) dynamometer (Interface- 6A68E, non-linearity, 0.04%, maximum capacity: Fx = Fy =10 kN, Fz = 20 kN, Mx =My = Mz = 500 Nm) was used. This dynamometer was able to simultaneously measure the time-histories of the forces and moments. The dynamometer was installed beneath the concrete flume floor by cutting the concrete flume floor, placing the device and re-embedding it as shown in Figure 3a and 3b.

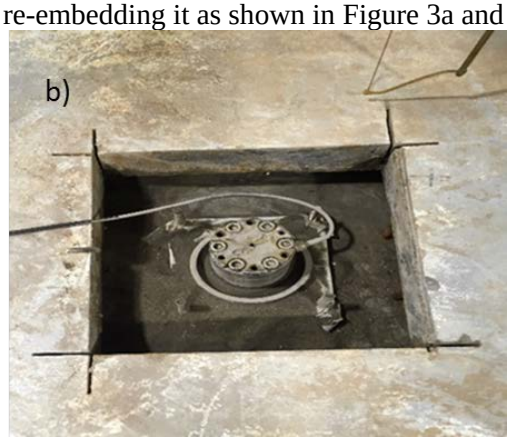

Figure 3. a) Dynamometer (Interface- 6A68E), b) Dynamometer embedded in the flume floor

A high-speed camera (HS, Flare 2M360-CL, sampling rate 70 Hz) was aimed towards the pipe from top to capture and analyze the bore impact with the pipe. A GoPro Hero4 Black was also installed 2 m upstream of the pipe and was used for observation purposes.

A steel pipe, referred to as the cylindrical pipe, with an outer diameter of 100 mm, a wall thickness of 5 mm and a length of 1400 mm was used in the experiments. The pipe was connected to the upper plate bolted to the dynamometer using two brackets, 2mm thick, made of steel as shown in Figure 1a.

2.2 Experimental program

The purpose of this study was to characterize hydrodynamic forces exerted on pipelines due to extreme flow events, modelled using a dam-break wave. A systematic and comprehensive experimental approach was conducted for this purpose. The most relevant parameters governing the problem at hand were varied during the experiments, namely: reservoir depth (h), tailwater depth (d), lower edge of pipe distance to bed (e) to diameter ratio (e/D) and pipe level of submergence (S) to pipe diameter ratio (S/D). (Figure 1c). Each test was repeated three times to assess the repeatability of the results of each test. Head ratio (d/h) is defined as the ratio between still water depth (d) and impoundment depth (h).

3. Results

3.1 Effect of dry bed VS wet bed conditions on water surface elevation

The effect of the dry bed versus wet-bed condition was investigated and analyzed. Figure 4 shows the water surface profile in dry and wet bed conditions measured by WG2 at x = 3.5 m. Good agreement of water surface time-histories was achieved between multiple repetitions for both dry and wet bed conditions. Normalized standard deviations (σ/h) of less than 5% for wet bed and less than 4 % for the dry bed were obtained

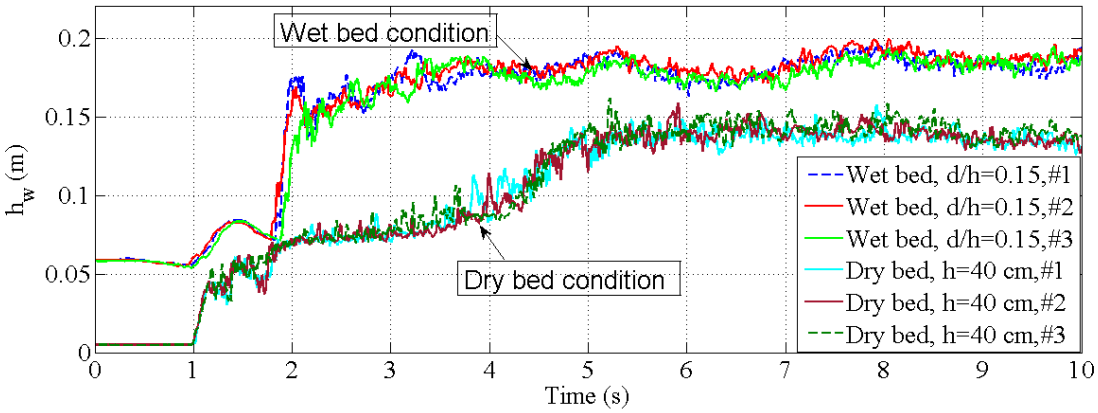

Fig. 4 Repeatability of tests for water level time history (WG2), dry and wet bed conditions.

In Figure 5, water surface profiles are plotted versus the dimensionless time, $t\sqrt{(g/h)}$. Experimental and Ritter′s theoretical solution were compared at the location of WG2 (x = 3.5 m) for three different impoundment depths h = 30, 40, and 50 cm. Figure 6 shows that, initially ($0< t\sqrt{(g/h)}<2$), the experimental results do not accurately match the Ritter [6] solution. This observed discrepancy is due to the fact that the surface roughness of the flume bed in the Ritter [6] solution is ignored (fully smooth bed). For the case of the dry bed conditions and at the beginning of dam-break wave surge, roughness plays a significant role as there is direct contact between bore front and flume surface. The experimental results agrees with a study conducted by Lauber and Hager [8] where the bed roughness was shown to have a significant role close to the wave fronts. They further concluded what other studies i.e., Wüthrich et al. [9] also found, that the Ritter's solution does not accurately represent the dam-break flow at the vicinity of the wave front as it does not consider the bed roughness in the suggested equation.

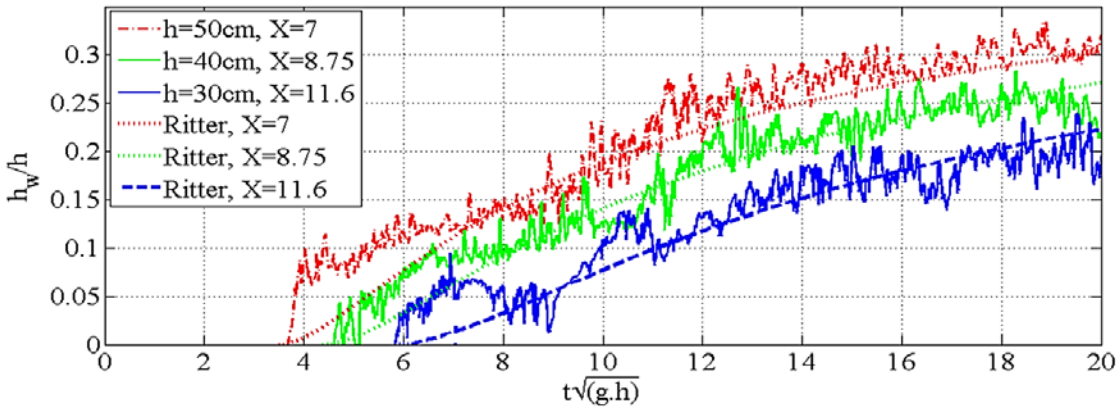

Figure 5. Non-dimensional dry bed condition water time-history surface profile: comparison with Ritter's [6] solution.

`Figure 6 illustrates the water surface profile for wet bed condition with impoundment depth of h = 40 cm and different still water levels (d) at the location of three wave gauges WG1 (a), WG2 (b) and WG3 (c). Reference time in the figure was the gate opening time. The figure shows earlier arrival time for the cases with smaller still water depth (wet bed condition) which indicates lager bore front celerity in such cases. The values recorded by WG2 and WG3 and shown in Figure 9(b) and 9(c) did not exhibit any change in the water surface profiles.

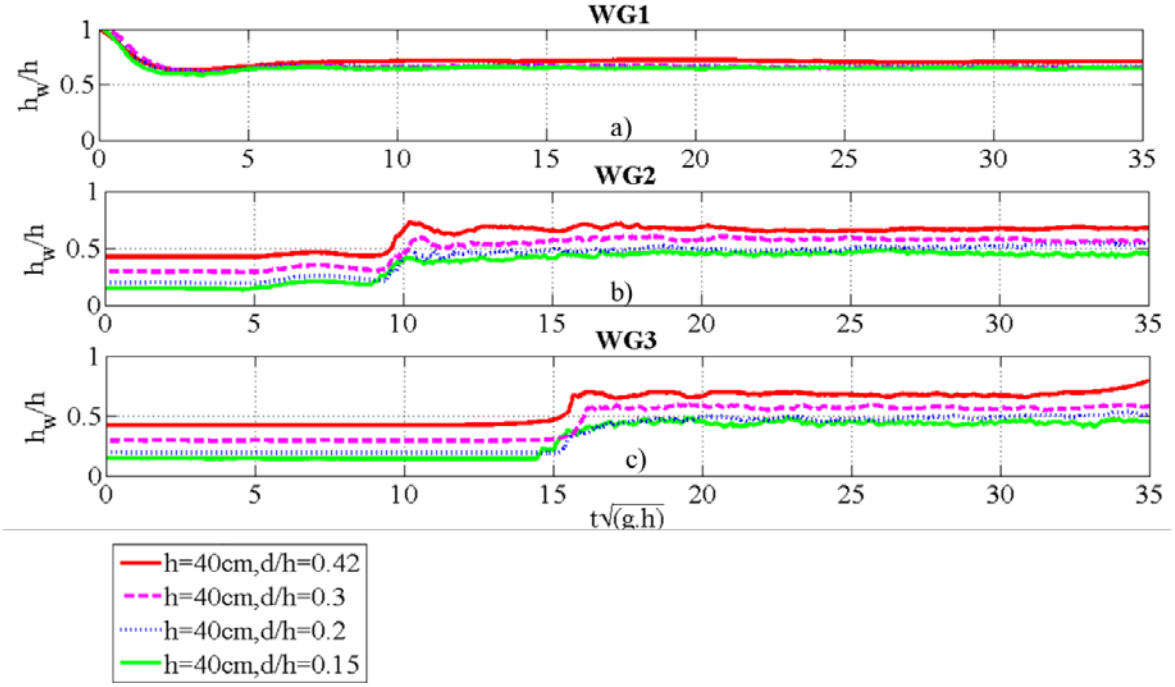

Fig. 6 Wet bed bore water surface time history. h=40 cm, different still water level, d=6, 8, 12, 17 cm, measured at location of a) Reservoir wave gauge (WG1) b) x=3.5 m (WG2) c) x=5.5m (WG3)

Figure 7 shows a comparison between dry bed and wet bed condition water surface time-histories. The data shows a steeper bore front and more abrupt water level rise in the case of the bore propagating over wet bed when compared to dry bed. Similar behaviour was found by several researchers, i.e. Nouri et al. [10] and Wüthrich et al. [9].

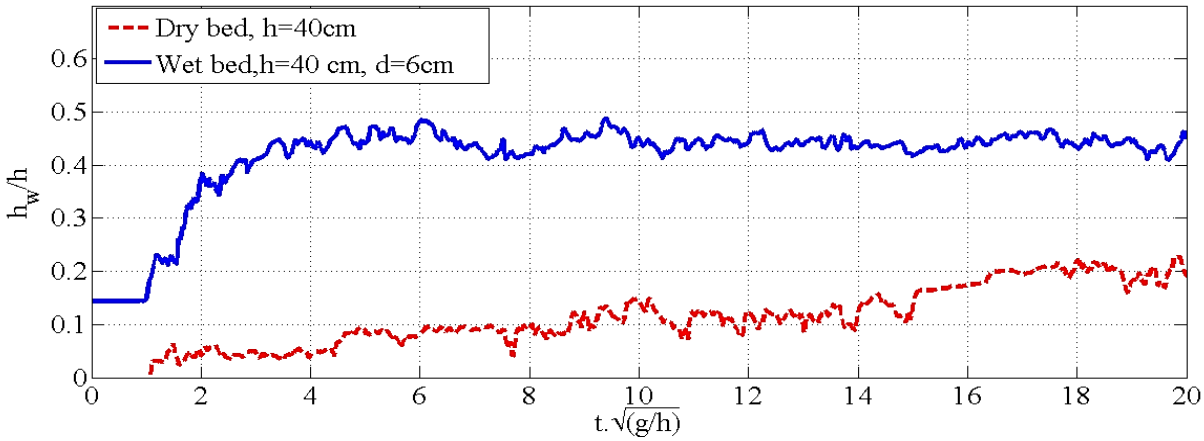

Fig. 7. Comparison between dry bed and wet bed condition normalized water depth time-history.

3.2 Effect of dry bed VS wet bed conditions on bore front velocity

For the case of dry bed conditions, the average front celerity of the propagating wave was estimated using the following ratio

$$U = \frac{\Delta x}{\Delta t} \tag{2}$$

where U is the bore front celerity in m/s. Δx is the distance between two wave gauges downstream of the gate, WG2 and WG3, and is equal to 2.1 m. Surge travel time is shown with Δt, as the time taken by the bore to travel between the two wave gauge measurements. A few previous studies have estimated bore front celerity (U) relative to impoundment depth (h) using:

$$U = \propto \sqrt{gh} \tag{3}$$

where α is a constant with various values reported in the literature. The constant value depends on flume hydraulic radius and roughness coefficient. Wüthrich et al., [9] suggests $\propto = 1.25$ while Matsutomi and Okatamo [11], suggest $\propto = 1.1$. Figure 8 shows results from the current study together with the previous studies mentioned above. This study suggests $\propto = 1.2$ as the constant in Equation 3.

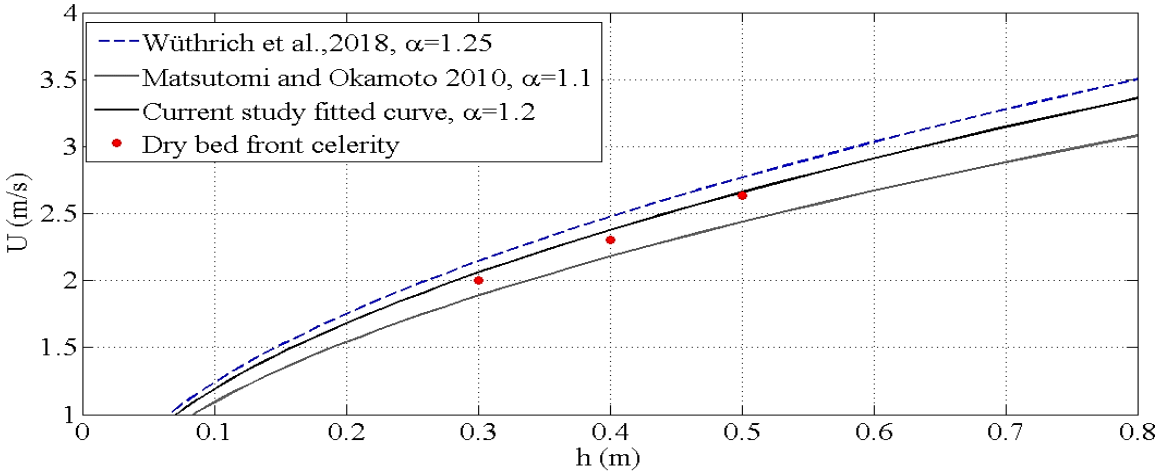

Fig. 8 Comparison between front celerity for dry bed in this study and previous studies

For the case of the wet bed velocities, bore front celerity was calculated using Equation (4) for different reservoir impoundment and downstream still water depths. Figure 9 illustrates the dimensionless bore front celerity versus head ratio (d/h) obtained from this study together with Chanson [5] empirical solution for bore front celerity for dam- break wave in horizontal channel initially filled with water as:

$$\frac{U}{\sqrt{gd}} = \frac{0.6345+0.3286\left(\frac{d}{h}\right)^{0.65167}}{0.00251+\left(\frac{d}{h}\right)^{0.65167}} \quad (6)$$

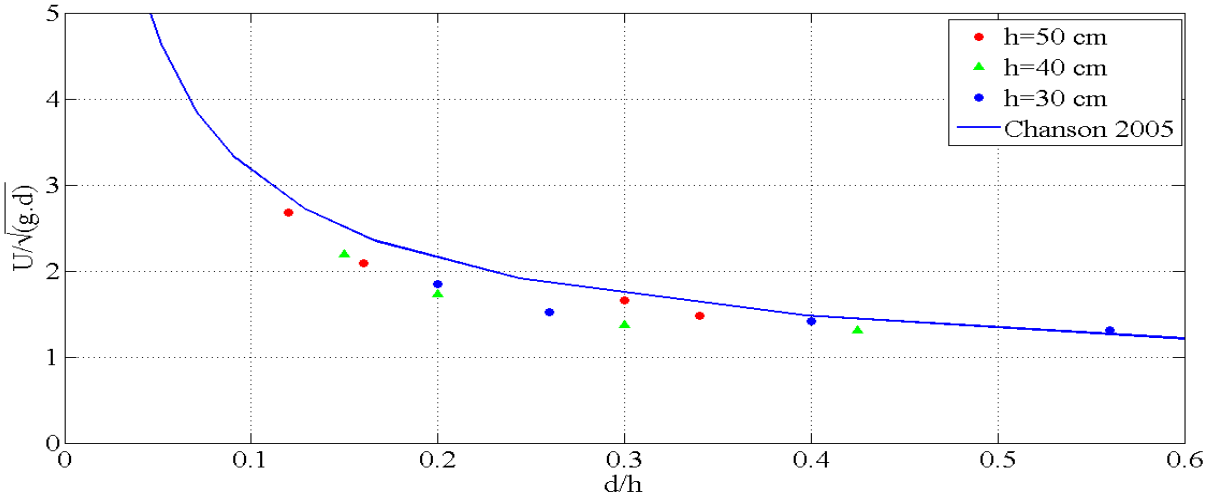

Fig. 9. Bore front celerity vs d/h. Solid line shows Chanson's (2005) solution while the points show experimental data

3.3 Drag and lift forces

Results from tests using different impoundment water depths and downstream of the gate still water depth values for different e/D values in wet and dry bed conditions are presented in the sections below. For clarity, all results are shown starting 1.0 seconds prior to the wave arrival time. Force magnitude in vertical (lift) and horizontal (drag) directions were set to zero shortly before the start each test to eliminate the effect of the latent hydrostatic forces as well as that of the pipe's own weight.

3.3.1 Force time-history for the dry bed condition

Figure 10 shows the results from a test conducted with a wave generated by an impoundment depth h = 40 cm in dry bed condition downstream of the rapidly opening gate. Figure 10a shows the water level time-history recorded by wave gage WG3 for the case with a gap ratio e/D=0.3, while Figures 10b and 10c show the time-history of the water level for e/D = 0.6 and 0.8 respectively. The schematic of the pipe with the corresponding distance from the bed is shown in Figures 10a, 10b and 10c, for e/D=0.8, 0.6, and 0.3 respectively, in order to visualize the level of the submergence and the full submergence time for each case. Water level for e/D = 0.3 rose rapidly immediately after the wave impact time while it gradually increased for cases with gap ratios of e/D = 0.6 and e/D = 0.8. Figure 10d shows the measured drag force time-history for the three gap ratios. In Figure 10d, one can observe that for e/D = 0.3, the drag force behavior was considerably different when compared to data obtained using other e/D ratios. For this particular value of e/D = 0.3, an impulse force at the wave arrival instant was recorded whereas for the other two gap ratios e/D no considerable such force was recorded. In the cases with large gap ratio (e/D = 0.6 and e/D = 0.8), water passed through the gap for the first few seconds of the wave propagation. However, in the case of smaller gap size (e/D = 0.3), less water passed through the gap and instead, a large portion of the incoming flow separated from the bed and surged on top of the pipe. This observation can also explain the sudden rise in the water level for e/D = 0.3 at t = 1.5 s (half a second after the wave arrival time). Hence, the impulse force was considerably larger for the test with e/D=0.3 while a longer rise time was observed for the force to reach its maximum value for the tests with e/D=0.6 and e/D=0.8. A smaller volume of the water passing through the gap and shorter rise time for the tests with e/D = 0.6 when compared to that in which e/D = 0.8, resulted in higher water level and larger drag forces at e/D = 0.6. For the test with e/D = 0.3, the water level reached the top edge of the pipe at t = 3.16 s. At this time, a surface roller formed right upstream of the pipe and started to propagate upstream causing a considerable decrease in the drag force.

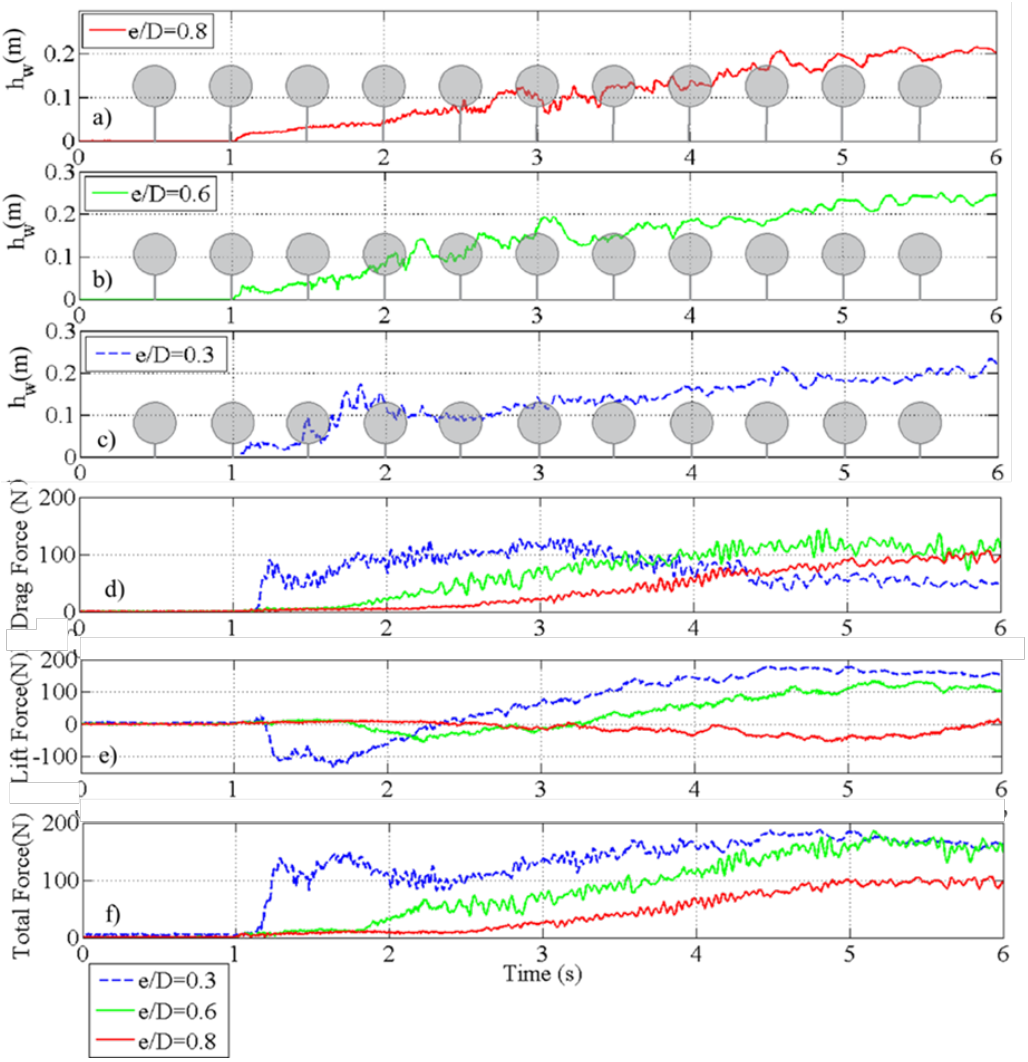

Fig. 10 Time-history of the water level and the drag and lift force component measurements, dry bed condition, impoundment depth h=40 cm a) water level, WG3, e/D=0.8, b) water level, WG3, e/D=0.6, c) water level, WG3, e/D=0.3, d) drag force time-history, e/D=0.3,0.6,0.8. e) lift force time-history, e/D=0.3,0.6,0.8. f) total force e/D=0.3,0.6,0.8.

3.3.2 Force time-history for the wet bed condition and different levels of pipe submergence

Figure 11 shows the results for the water depth, the drag force, lift force and the total force for different still water level depths downstream of the gate for the case of e/D = 0.6. d/h ratio was adjusted by varying the still water depth (d) and using a constant impoundment depth (h,) which resulted in different levels of pipe submergence (S/D) as shown in Figure 11a.

The time history of the drag force (Figure 11b) shows that for S/D = 0 (the pipe not being submerged at the initial stage before opening the gate), the drag force initially exhibited an initial bore impact (impulse force) and further decreased to lower magnitudes afterwards. When the initial still water level was below the bottom edge of the pipe (d/h = 0.075), the measured run-up force was larger compared to the impulse force just a few seconds after the bore impact. However, when the pipe was partially submerged with S/D < 0.5, the impulse force was the maximum one. For S/D ≥ 0.5, a smaller impulse force was observed and the magnitude of the drag force remained constant as the pipe became fully submerged. In the case of a fully submerged pipe with S/D=1, no considerable impulse force was recorded and a gradual drag force magnitude increase was observed, mainly due to an increase in the flow velocity. The run-up force was caused by the

pipe obstructing the flow. Therefore, as the pipe was increasingly submerged, this force decreased. This occurred faster for the pipe with a larger initial level of submergence.

The time history of the lift force shown in Figure 11c, indicates a decrease in this force's magnitude with an increase in the still water depth downstream of the gate and, as a result, an increase in the initial S/D ratio. Lowest values were observed for the case of the fully submerged pipe (S/D=1). In the case of a fully submerged pipe, incoming flow only passed over the top of the pipe inducing small, mostly downward, vertical forces. Downward lift force at the time of the bore impact for the cases when S/D=0 is due to the volume of water surging on top of the pipe at the time of bore impact. The rapidly-surging water further pushed the pipe downwards. Figure 11d shows the decrease in the total force time history with an increase in the d/h ratio and an increase in the downstream still water depth. As discussed in the companion paper Part 1, a significant decrease in flow velocity was observed as the downstream still water level was increased. This explains the smaller force component magnitudes in larger d/h ratios.

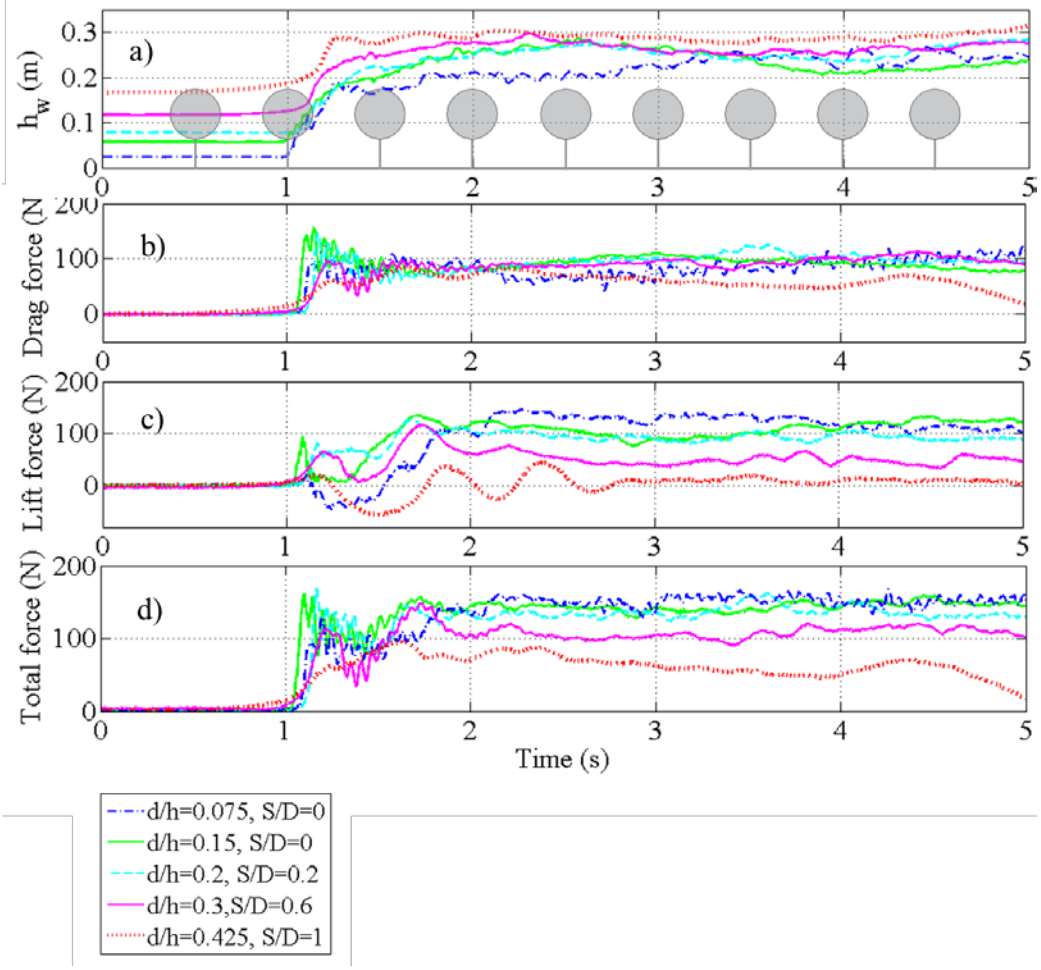

Fig. 11 Time-history of the water level and force component measurements, wet bed condition, different d/h ratios (d/h = 0.075, 0.15, 0.2, 0.3, 0.425) , e/D=0.6 a) water level, WG3, b) drag force time history c) lift force time history d) Total force.

3.3.3 Force coefficients

Force coefficients are used to determine the drag and lift forces exerted on a body placed within flow. Current design guidelines recommend force coefficient values for different bodies including horizontal cylinders exposed to steady flow conditions. For the case of unsteady flow conditions, force coefficients have been suggested mostly for vertically-oriented bluff bodies. For the first time, this research investigates the variation of force coefficients for horizontal cylinders placed in unsteady flow conditions (dam-break waves). Due to the unsteady nature of the dam-break flow, force coefficients are not constant but vary considerably over the duration of the flow-structure interaction. In this study, the measured horizontal force

incorporates both the hydrodynamic and hydrostatic components. Therefore, the term "resistance coefficient", rather than "drag coefficient" was used for the experimentally-determined horizontal force coefficient similar to studies for steady flows around bridge piers and for tsunami impacts on vertical structures. The resistance coefficient for different pipe configurations, different impoundment depths and different wet bed conditions downstream of the gate, were calculated using:

$$C_R = \frac{2F_H}{\rho L D u^2} \tag{4}$$

where F_H is the measured horizontal force during the experimental work; D and L are the pipe diameter and pipe length, respectively and u is the average free stream velocity.

Lift coefficients were calculated using:

$$C_L = \frac{2F_z}{\rho D L u^2} \tag{5}$$

where F_Z is the measured vertical force.

Figures 12 illustrates relationships for the calculated resistance coefficient values as a function of the Froude number for the experiment. The values of the maximum estimated resistance coefficients were used to determine an upper envelope for the resistance coefficient, C_r. In the case of the dry bed condition, due to the higher flow velocities, the values of the resistance coefficients are found at the right side of the graph, corresponding to the larger Froude numbers which characterized the dry bed condition. Based on the results presented in Figure 12, the suggested C_r values vary between 1.0 and 3.5. Figure 12 shows that, for the case of supercritical flows (Fr > 1), C_r values were almost constant, while they linearly increased with a decrease in Fr number in the transitory and subcritical flow regime (Fr < 1). The black line in Figure 12 represents the upper envelope encompassing the entire range of experimental cases performed, from subcritical to supercritical flow conditions. As shown, it covers a variety of submergence conditions and gap space, as well as both wet and dry bed conditions.

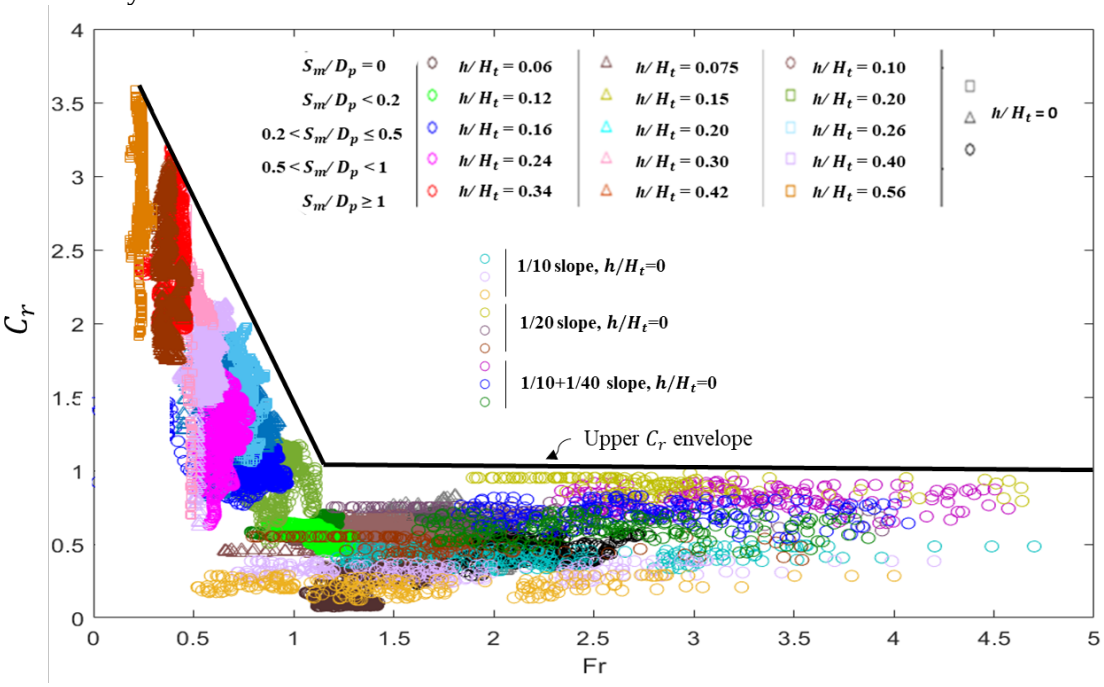

Fig. 12 Calculated resistance coefficient vs. Froude number for all the experimental cases tested

Similar to the resistance coefficient, Figure 13 presents the experimentally determined lift coefficients were plotted against the calculated Froude numbers.

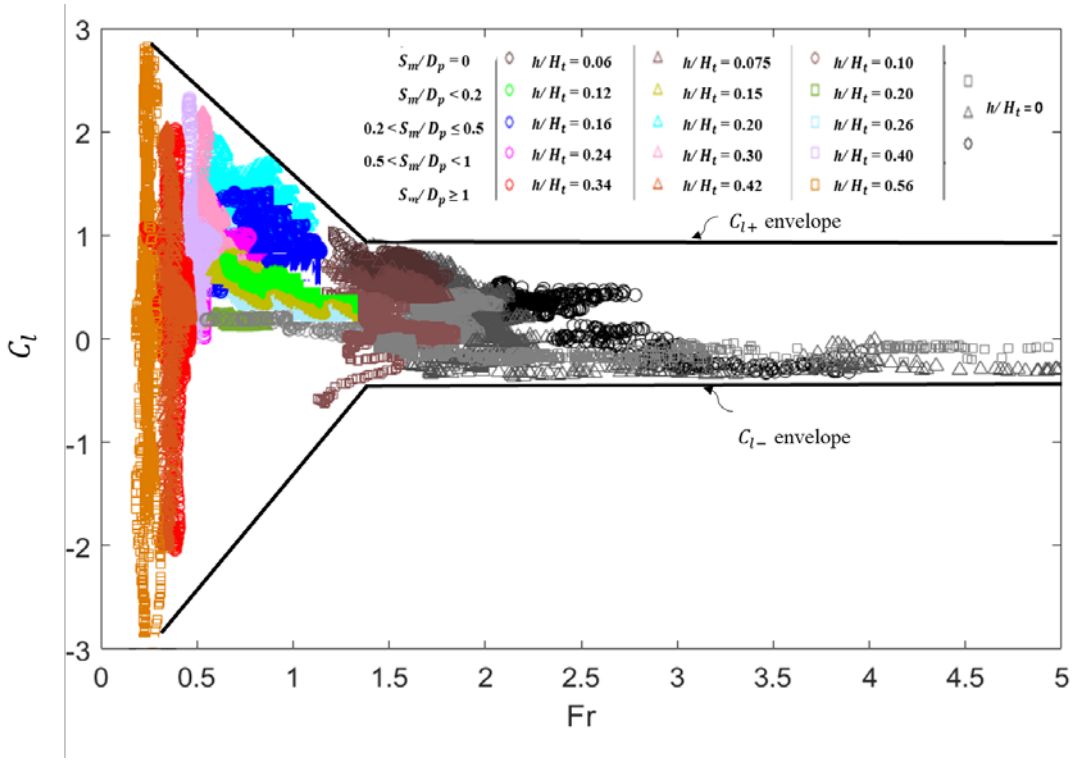

Fig. 12 Calculated lift coefficient vs. Froude number for all the experimental cases tested

The maximum upward and downward lift coefficients for all experimental cases were calculated to determine two envelopes which encompassed the variation of these coefficients with the Froude number. The values of the upward lift coefficient, C_{l+} for pipelines subjected to unsteady flow conditions vary in the range of $1.0 \le C_{l+} < 2.8$ while those of the downward lift coefficient, C_{l-} vary in the range of $-2.8 \le C_{l-} < -0.5$. Similar to the resistance coefficient behavior, the upward and downward lift coefficients remained almost constant in the supercritical flow region, while their absolute values increased as the value of Fr decreased in the transitional and subcritical flow region.

4. Conclusions

A comprehensive experimental program was conducted to investigate the mechanisms of the extreme hydrodynamic loading exerted on a pipe due tsunami-like hydraulic bore flows. The time-history of the hydrodynamic forces exerted on the pipe was measured and analyzed for different experimental conditions with respect to the pipe installation (distance/gap from the bed) as well as the flow characteristics (degree of submergence and hydraulic bores with different heights as well as dry vs. wet bed conditions over which the bore propagated. Finally, resistance and lift coefficients have been calculated for a wide variety of experimental conditions.

5. References

[1] ASCE/SEI (ASCE/Structural Engineering Institute). Minimum design loads and associated criteria for buildings and other structures. ASCE/ SEI 7-16, Reston, 2017, VA, 25-50.

[2] Rossetto, T.; Peiris, N.; Pomonis, A.; Wilkinson, S.M.; Del Re, D.; Koo, R.; Gallocher, S. The Indian Ocean tsunami of December 26, 2004: observations in Sri Lanka and Thailand. *Natural Hazards*. 2007 Jul 1;42(1). 105-24

[3] Fritz, H.M.; Phillips, D.A.; Okayasu, A.; Shimozono, T.; Liu, H.; Mohammed, F.; Skanavis, V.; Synolakis, C.E. and Takahashi, T., The 2011 Japan tsunami current velocity measurements from survivor videos at Kesennuma Bay using LiDAR. *Geophysical Research Letters*, 2012, 39, Vol. 7.

